

See discussions, stats, and author profiles for this publication at: <https://www.researchgate.net/publication/264797379>

Oxidized Multiwalled Carbon Nanotubes as Antigen Delivery System to Promote Superior CD8 + T Cell Response and Protection against Cancer

ARTICLE *in* NANO LETTERS · AUGUST 2014

Impact Factor: 13.59 · DOI: 10.1021/nl502911a · Source: PubMed

CITATIONS

4

READS

96

9 AUTHORS, INCLUDING:



[Luara Isabela dos Santos](#)

University of Oxford

6 PUBLICATIONS 30 CITATIONS

[SEE PROFILE](#)



[Joao Paulo Coelho](#)

Complutense University of Madrid

5 PUBLICATIONS 5 CITATIONS

[SEE PROFILE](#)



[Marcos A Pimenta](#)

Federal University of Minas Gerais

243 PUBLICATIONS 12,022 CITATIONS

[SEE PROFILE](#)



[Dawidson A Gomes](#)

Federal University of Minas Gerais

65 PUBLICATIONS 1,082 CITATIONS

[SEE PROFILE](#)

Oxidized Multiwalled Carbon Nanotubes as Antigen Delivery System to Promote Superior CD8⁺ T Cell Response and Protection against Cancer

Paula Cristina Batista de Faria,^{†,‡,○} Luara Isabela dos Santos,^{†,§,○} João Paulo Coelho,^{||} Henrique Bücker Ribeiro,[†] Marcos Assunção Pimenta,[#] Luiz Orlando Ladeira,[#] Dawidson Assis Gomes,[§] Clascídia Aparecida Furtado,^{*,||,○} and Ricardo Tostes Gazzinelli^{*,†,§,▽,○}

[†]Instituto de Pesquisa René Rachou, Fundação Oswaldo Cruz, 30190-002 Belo Horizonte, MG Brazil

[‡]Instituto de Genética e Bioquímica, Universidade Federal de Uberlândia, 38400-902 Uberlândia, MG Brazil

[§]Departamento de Bioquímica e Imunologia, Universidade Federal de Minas Gerais, 31270-001 Belo Horizonte, MG Brazil

^{||}Centro de Desenvolvimento da Tecnologia Nuclear, CDTN/CNEN, 31270-001 Belo Horizonte, MG Brazil

[†]Mackgraphe, Universidade Presbiteriana Mackenzie, 01302-907, São Paulo, SP Brazil

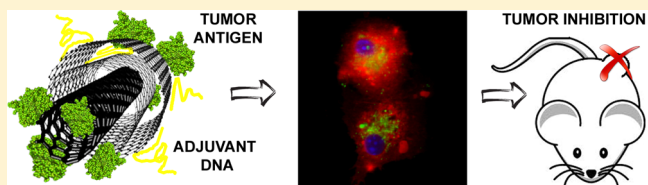
[#]Departamento de Física, Universidade Federal de Minas Gerais, 31270-001 Belo Horizonte, MG Brazil

[▽]Division of Infectious Diseases and Immunology, University of Massachusetts Medical School, Worcester, Massachusetts 01605, United States

Supporting Information

ABSTRACT: Properties like high interfacial area with cellular membranes, unique ability to incorporate multiple functionalization, as well as compatibility and transport in biological fluids make carbon nanotubes (CNTs) useful for a variety of therapeutic and drug-delivery applications. Here we used a totally synthetic hybrid supramolecule as an anticancer vaccine formulation. This complex structure comprises CNTs as delivery system for the Cancer Testis Antigen named NY-ESO-1, allied to a synthetic Toll-Like Receptor agonist. The CNT constructs were rapidly internalized into dendritic cells, both *in vitro* and *in vivo*, and served as an intracellular antigen depot. This property favored the induction of strong CD4⁺ T as well as CD8⁺ T cell-mediated immune responses against the NY-ESO-1. Importantly, the vaccination significantly delayed the tumor development and prolonged the mice survival, highlighting the potential application of CNTs as a vaccine delivery system to provide superior immunogenicity and strong protection against cancer.

KEYWORDS: Nanovaccine, carbon nanotubes, NY-ESO-1, cancer, CD8+ activation



The peculiar sizes and shapes of nanoparticles endow them with properties that can be very useful in biomedical applications. Nanomedicine has been explored to overcome some limitations of the approaches currently used in order to optimize the delivery of antigens and increase the efficacy of vaccines toward a more selective and effective way.^{1,2}

Carbon nanotubes (CNTs) are of particular interest for vaccine development, as they are not immunogenic and as delivery vector should induce strong and long-lasting antigen-specific humoral and cellular immune responses.^{3,4} Among their intrinsic properties these nanosized particles have the ability to interact to or cross biological membranes and deliver biomolecules into the cytoplasm.¹ In addition, the characteristic of extremely high surface area to volume ratio confers to CNTs the capacity to provide multiple attachment sites for various bioactive molecules such as peptides,^{3–5} proteins,^{6,7} nucleic acids,^{8–11} and drugs^{12–14} and therefore to generate hybrid supramolecules of high specificity and selective biological

function. Moreover, CNTs can protect the attached molecules against enzymatic degradation¹⁵ resulting in a superior intracellular biostability and providing a depot effect,^{3,8} allowing enough time for migration and boost lymphocytes and consequently to induce a long-lasting immune response.

Optimally designed cancer vaccines should combine the best tumor antigens with the most effective immunotherapy agents and/or delivery strategies to achieve positive clinical results.¹⁶ Currently, vaccine formulations against experimental tumors and other diseases have already been tested, combining protein antigens with Toll-Like Receptor (TLR) agonists, which act as immunological adjuvants. This strategy enhances the ability to activate dendritic cells (DCs), favoring antigen cross-presentation and then the development of a strong CD8⁺ T cells and Th1 lymphocyte-mediated immunity.^{17,18} Because of

Received: July 29, 2014

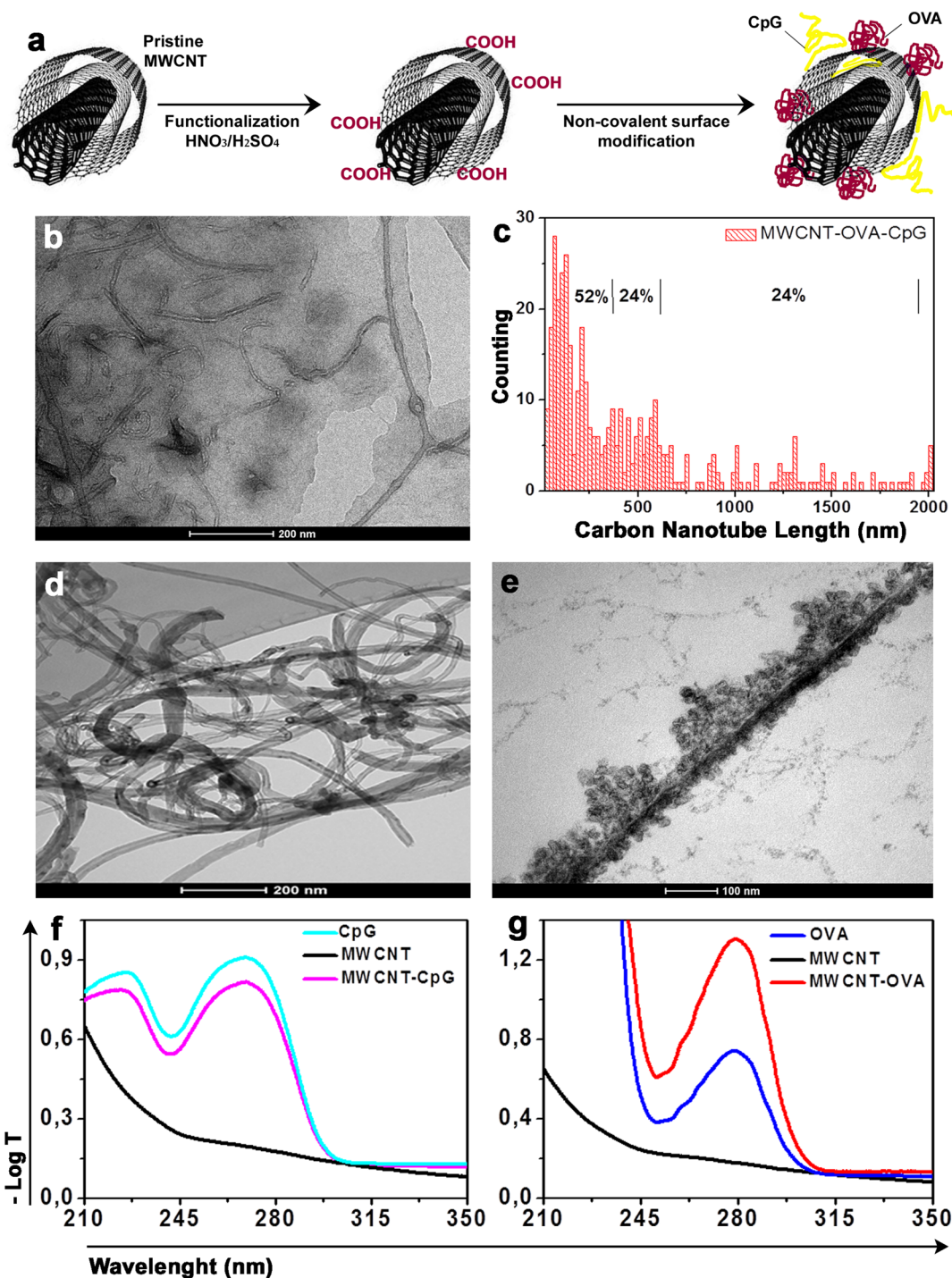


Figure 1. Noncovalent immobilization of the biological entities on the oxidized multiwalled carbon nanotubes (MWCNTs). (a) Schematic diagram showing the strategy for preparation of MWCNT-based delivery systems. (b) Transmission electronic microscopy images of shortened MWCNT in vaccine formulation. (c) Histograms for the statistical analysis of nanotube length distribution. (d) TEM image of oxidized MWCNT. (e) TEM images of the MWCNT-OVA complex showing the patterned assembly of OVA entanglements on oxidized nanotube surface. (f) Absorbance spectra in the UV region for oxidized MWCNT, CpG, and MWCNT-CpG complex. (g) Absorbance spectra in the UV region for oxidized MWCNT, OVA, and MWCNT-OVA complex. To estimate the percent of hypo- and hyperchromism effects, the absorbance due to oxidized MWCNTs was subtracted from the spectra of MWCNT-CpG and MWCNT-OVA.

restricted expression in normal tissues, cancer testis (CT) antigens represent particularly interesting candidates for immunotherapy of cancer.¹⁹ NY-ESO-1 is a CT antigen that is expressed in a variety of human cancers including melanoma, breast, lung, prostate tumors, and others,^{20,21} being highly immunogenic and able to induce T cell-mediated immun-

ity.^{22,23} Consistently, immunotherapy has shown promise in several early phase clinical trials involving NY-ESO-1-expressing tumors in humans.^{24,25}

Here, we report that both prophylactic and therapeutic strategies are highly effective when employing CNTs as delivery system for an anticancer vaccine formulation. This antitumor

vaccine was composed of NY-ESO-1 as antigen and CpG oligonucleotides (CpG-ODNs), a TLR9 agonist, as immunological adjuvants, both attached noncovalently to oxidized multiwalled CNTs (MWCNTs). Our findings showed that the MWCNT constructs were rapidly internalized into DCs and were highly efficient in inducing both humoral as well as CD4⁺ T and CD8⁺ T cell responses that effectively controlled melanoma growth in antigen-specific manner.

Noncovalent Immobilization of Biomolecules on the MWCNT Surface. To test the efficiency of MWCNTs as an antigen delivery system, they were initially coupled to ovalbumin (OVA), a standard antigenic protein that is widely used in immunological studies. In addition, CpG-ODNs were associated with the MWCNT as immunological adjuvant that potentiate the T cell mediated immune responses.

The surface chemistry and size of carbon nanotubes play critical roles in enhancing their compatibility with the biological medium, changing their toxicity and regulating their interactions with cells and biological molecules.²⁶ Oxidation in mixtures of sulfuric and nitric acids is known to produce shortened CNTs containing oxygenated groups along the sidewalls and extremities of the tubes.^{27,28} These functional groups provide hydrophilicity to the tubes allowing the preparation of stable dispersions in water, buffer solutions, and culture media. As shown in Figure 1a, this was the first step of our approach to link immunogenic proteins and the TLR9 agonist to MWCNTs surface. Pristine MWCNTs were purified and oxidized in subsequent thermal and acid treatments. A purity degree of 95 wt % of carbonaceous materials was achieved as estimated by thermogravimetry. The oxidized MWCNTs were dispersed in water by tip sonication at an initial concentration of 0.25 mg·mL⁻¹. A centrifugation step to remove longer and nondispersed carbonaceous materials was performed at 1700g for 60 min. After oxidation/dispersion/centrifugation processes, we obtained a stable 0.12 mg·mL⁻¹ aqueous dispersion of shortened MWCNTs functionalized with close amount of carboxylic acids (0.8 mmol·g⁻¹) and phenols (0.9 mmol·g⁻¹) distributed at the ends and walls of the tubes. The final concentration was estimated by establishing the absorptivity of the MWCNT in a UV-vis absorbance calibration curve. The amount of each –COOH or –OH group, quantified by acid–base potentiometric titration, corresponds to approximately two functional groups in every 100 carbon atoms.

For the vaccine formulation, 10 µg of the protein antigens (OVA or NY-ESO-1) and 18 µg of CpG-ODNs were solubilized in a certain volume of aqueous dispersion containing 20 µg of oxidized MWCNTs, forming nonspecific MWCNT-antigen-CpG constructs stably dispersed in aqueous medium. The dispersion was diluted to 100 µL with PBS buffer solution.

The morphology and length distribution of the MWCNT in the MWCNT-OVA-CpG formulation were characterized by transmission electron microscopy (TEM). Figure 1b shows a TEM image illustrating the general aspect of the shortened tubes. Similar TEM images from different regions are displayed in Supporting Information Figure S1 probing that this pattern is representative of the whole sample. The nanotube length distribution was statistically measured in several of those TEM images. The histogram in Figure 1c shows that 48% of the tubes are below 250 nm (76% below 600 nm).

The kinetics curve of adsorption of the OVA model antigen on the oxidized MWCNTs shows that 0.5 mg of OVA was adsorbed by 1 mg of MWCNTs in 45 min and a saturation of

0.8 mg of OVA adsorbed by 1 mg of MWCNT was reached after 90 min (Supporting Information Figure S2). This behavior indicates that for the 1:2 OVA/MWCNT weight ratio used in our formulation, a very large amount of (or virtually any) protein should be adsorbed on the nanotube surface, even in a thermodynamic equilibrium with CpG oligonucleotides.²⁹ These results are corroborated by Zeta potential measurements of the MWNT-biomolecules dispersions.

Electrostatic repulsion between ionizable molecules adsorbed on carbon nanotubes is one of the mechanisms of stabilization of nanotube colloids. The stabilizing effect is proportional to the surface charge on the nanotube. The magnitude of this charge can be measured in the form of the Zeta potential, ξ , the electrical potential at the edge of the coated colloid. Colloidal particles with $|\xi| > 15$ mV are expected to be stable.³⁰ Hence, to achieve stable dispersions of CNT–biomolecules complexes, ξ should be maximized. ξ values of -26, -35, and -52 mV were estimated for the oxidized MWCNT dispersion and OVA and CpG solutions, respectively, all prepared in physiological pH. For dispersions of MWCNT-OVA and MWCNT-CpG complexes, isolately prepared, the absolute values of ξ were found to be -34 and -46 mV, respectively, evidencing the dispersing role of both biomolecules and a high stability of those dispersions. The similarity of the ξ values for OVA solution and MWCNT-OVA complex dispersion also evidence that the MWCNT surface should be densely coated by the protein. For the MWCNT-OVA-CpG constructs, the average ξ value of -42 mV is in between the ξ values for MWCNT-OVA and MWCNT-CpG complexes, showing that the dispersion stability of the MWCNT constructs should be a balance of the magnitude of electrostatic repulsive forces between all the biomolecules adsorbed on the nanotube surface.

TEM images of the protein-coated MWCNT illustrate the adsorption and the Zeta potential results. A film of organic molecules involving the nanotubes shown in Figure 1b reveals the change in the MWCNT surface environment in the presence of the biomolecule. This film was not observed in the images of the oxidized MWCNT itself (Figure 1d). A better view of this environment with details of the assembly of OVA entanglements on the MWCNT surface can be seen in Figure 1e. We can see a first layer of protein covering the oxidized MWCNT surface and agglomerates of OVA entanglements patterned adsorbed onto this layer. The average spacing between the protein agglomerates was measured up to ~100 nm, as described before in AFM studies of nonspecific binding of BSA on SWCNT.^{7,29}

The nature of the interactions between the oxidized MWCNT and the biomolecules in the MWCNT-OVA and MWCNT-CpG complexes were characterized by optical absorption spectroscopy. Figure 1f shows the absorbance spectra in the UV region for CpG, oxidized MWCNT and MWCNT-CpG dispersions. While the spectrum of the oxidized MWCNT is characterized by the continuous π -plasmon absorbance, a prominent absorption band between 240 and 290 nm was observed in the spectrum of the CpG due to the overlapping of in-plane $\pi-\pi^*$ transition peaks from the CpG bases, such as thymine (205 and 265 nm), cytosine (212, 228, and 269 nm), and guanine (199, 248, and 275 nm).³¹ After introducing the CpG in the MWCNT dispersion, a hypochromic effect (~12%) of this band was observed. This effect, typical of π -stacked chromophores, is expected to occur for nucleotides dipole transitions that lie along the axis of the

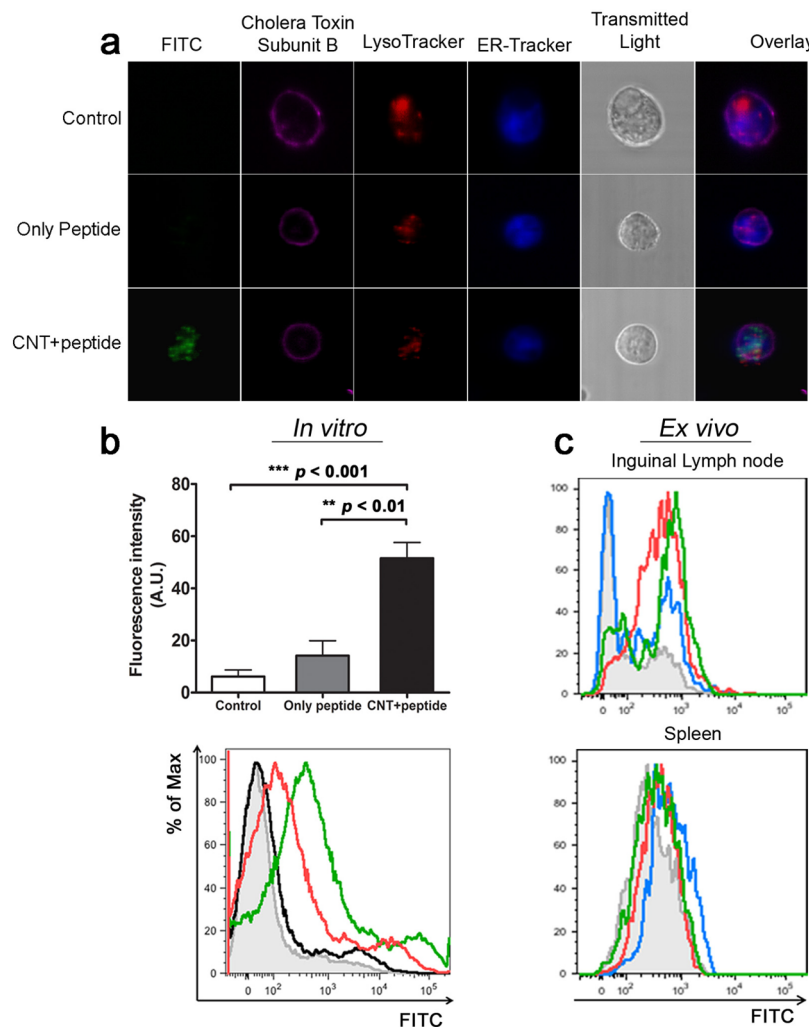


Figure 2. Uptake of the multiwalled carbon nanotubes (MWCNTs) constructs by DCs. (a) Live-cell confocal fluorescence microscopy images of untreated dendritic cells (DCs) (top), or loaded with FITC-labeled OVA peptide only (middle), and with MWCNT-peptide complexes (bottom). Intracellular peptide (green), plasmatic membrane (pink), lysosomes (red), and endoplasmatic reticulum (blue) were stained. (b) Optical intensities of randomly selected cells from each sample in panel a. Flow cytometric analysis of the internalization into DCs. DCs without antigen (shadow), and DCs pulsed with MWCNT only (black), peptide-FITC only (red), or MWCNT-peptide-FITC complexes. Error bars, standard errors of the mean. (c) MWCNT-peptide-FITC were injected subcutaneously and the presence of intracellular constructs in dendritic cells at 1 h (green), 20 h (red), and 3 days (blue) postinjection were evaluated by flow cytometry.

anisotropic CNT and confirm the adsorption of the CpG on the oxidized MWCNT surface with the interactions strength being provided predominantly by π -stacking.^{32,33} An opposite effect was however observed for MWCNT-OVA complex. Figure 1g shows the appearance of a hyperchromic effect of ~60% in the OVA absorption band after interaction with the oxidized MWCNT relative to the noninteracted OVA. The absorption bands between 260 and 300 nm are a superposition of transition peaks from the aromatic amino acids, tyrosine (268 and 277 nm), and tryptophan (285 nm). This hyperchromicity could occur for different transition directions, which induce a dipole in the same direction in the paired structure, or for stacked structures with transitions perpendicular to the plane of the chromophores (such as n- π^* transitions of zwitterionic amides).³⁴ Therefore, the hyperchromism effect suggests a predominant electrostatic character for the interaction between acid oxygenated groups on the nanotube surface and base groups in the protein. An electrostatic interaction was also characterized between carboxylated CNTs and bovine serum albumin (BSA) protein

by fluorescence spectroscopy³⁵ and between carboxylated CNTs and the arginine amino acid by theoretical studies.³⁶

Delivery of MWCNT-Peptide Complex into DCs. We examined cellular uptake of oxidized MWCNT alone and conjugated with FITC-labeled OVA-derived K^b-SIINFEKL 257–264 peptide (OTI). Figure 2a shows confocal fluorescence microscopy images of phagocytic DCs after treatment with 20 $\mu\text{g}\cdot\text{mL}^{-1}$ of MWCNT or MWCNT-OTI-FITC conjugates for 24 h at 37 °C. The presence of MWCNT in the cytoplasm, mainly distributed in the perinuclear region of DCs, shows the phagocytic ability and the functional viability of these cells, as previously reported for same-sized single walled CNTs.³ We could observe colocalization between the nanotubes and the fluorescent peptides, confirming the efficacy of the attachment previously characterized for the model antigen. Moreover, we observed a significant enhancement of the fluorescence inside the cells loaded with MWCNT-OTI complex, when compared to those with the peptide alone (Supporting Information Figure S3a).

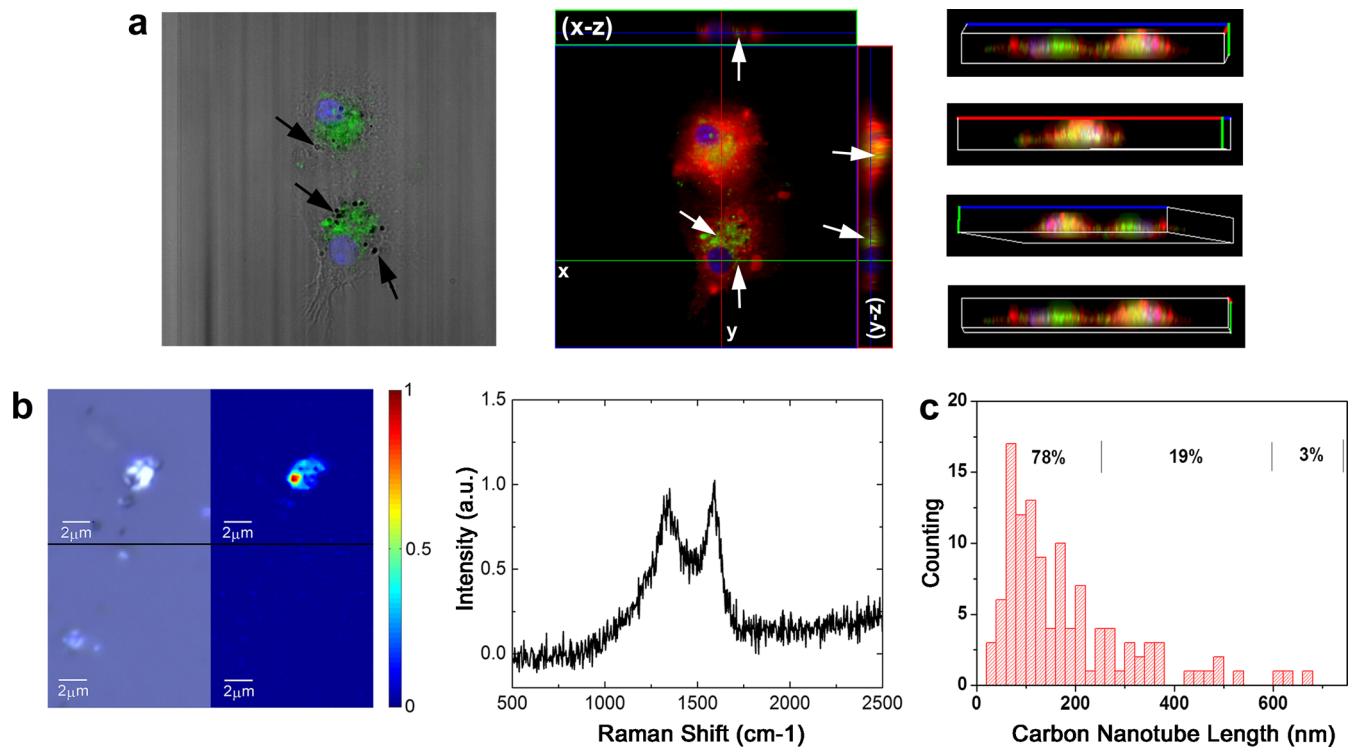


Figure 3. Intracellular localization of the MWCNTs constructs. (a) Confocal immunofluorescence images 20 h after incubation with MWCNT-peptide-FITC. Labeled peptide is in green and the nucleus is stained with DAPI (blue). Internalized carbon nanotubes are indicated in DIC and fluorescence merge in first panel (black arrows). Top and side views of a representative Z-stack confocal image (merge of 16 slices with 0.7 μm of thickness) from MWCNT-peptide-FITC complex into DCs are shown in second and third panels, respectively. Serial optical sections were collected for three-dimensional reconstruction; $x-z$ sections are shown at the top, and $y-z$ sections are shown at the right of image. Note that there is an accumulation of peptide near of the nuclear region (white arrows). Images were collected using 488 nm laser. (b) Optical image (left side) and Raman image of the nanotube G-band (right side) in a region containing one cell with and another cell without MWCNT, respectively, recorded with the 532 nm laser line. (c) Histograms for the statistical analysis of nanotube length distribution of those found within dendritic cells evaluated by TEM.

Although the mechanism for the internalization of CNTs into cells has not been fully established (endocytic or needle-like penetration), it is generally recognized that CNTs are able to enter various biological membrane barriers,¹ but this largely depends on their length and surface chemistry.^{37,38} Live-cell confocal microscopic images showed that the majority of FITC fluorescence is colocalized with the endolysosomal compartment marker, indicating that antigen-nanoparticle complexes were internalized through endocytosis (Figure 2a). This is consistent with reported observations that confirm that well-dispersed carbon nanotubes transporting proteins or oligonucleotides are internalized into living cells via energy-dependent endocytosis.^{7,38} These findings strengthen the idea that the attachment of antigens onto carbon nanotubes surface greatly enhances the delivery of antigens to a degradative perinuclear region into the cytosol, leading to improved antigen presentation in competent cross-presenting cells.^{3,39}

Flow cytometry analyses on treated live cells are consistent with the confocal microscopic observations. Internalization could be observed through an increase in side-scatter intensity with MWCNT-OTI-FITC conjugate confirming that peptide was taken up by DCs much more efficiently when attached to the nanotubes (Figure 2b). We also observed that in the secondary lymphoid tissues, dendritic cells were the main source of intracellular MWCNTs constructs at 1 h (inguinal lymph nodes) and 3 days (spleen) post subcutaneous injection (Figure 2c). Thus, we conclude that after uptake of MWCNT-antigen complex, dendritic cells followed by macrophages (but

not NK, B, or T cells) drained into secondary lymphoid tissue⁴⁰ permitting premature antigen presentation⁴¹ and then activating resting T cells (Supporting Information Figure S4).

To more minutely characterize the uptake of antigen-coated MWCNTs, we perform series of planes through the thickness of two separated DCs. The nucleus and the cytoplasmic membrane were stained with DAPI and Cell Mask (Life Technologies), respectively. Top and side views of the three-dimensional reconstruction (3D) allow the visualization of the nanotubes and fluorescent peptides into treated cells (Figure 3a). A 3D reconstruction video of confocal microscopy images is available as Supporting Information. To this end, we also confirm the intracellular localization of protein-coated MWCNTs by a combined optical microscopy and Raman spectroscopy analysis. We could observe the greater concentration of G-band Raman intensity inside the cell, pointedly identified in the optical image. It is known that the G-band intensity in Raman spectra can be directly correlated to the nanotube concentration in the sampled region.⁴² No signal was detected in control cells without MWCNTs (Figure 3b). Hence, functionalized MWCNTs were effectively recognized and taken up by dendritic cells. Furthermore, TEM images of the same cell preparation indicate a preference of dendritic cells for internalization of shortened nanotubes. About 80% of those found inside cells have length up to 300 nm (Figure 3c).

To assess the DCs viability exposed to functionalized MWCNTs, two different assays were performed. Cellular toxicity was evaluated by the lysosomal incorporation of the

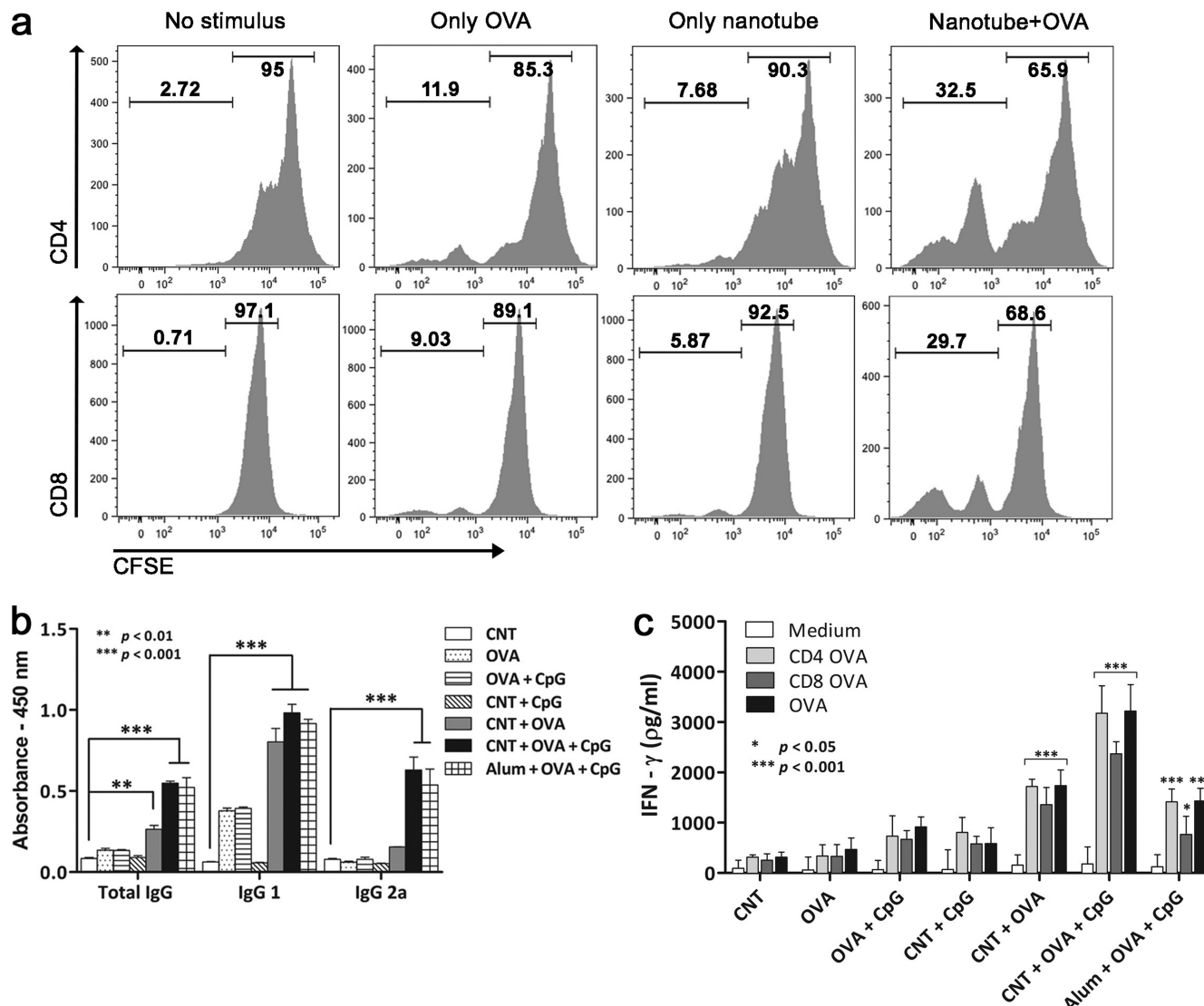


Figure 4. Carbon nanotubes increased the efficiency of cross-presentation of OVA in vitro and induced a specific immune response in vivo. (a) In vitro mouse lymphocyte proliferation measured using CFSE labeling and flow cytometric analysis. (Left) CFSE-labeled pattern of control nonproliferating cells in culture without any stimulus. (Right) Both CD4⁺ and CD8⁺ T cells proliferation and consequently cross-presentation of OVA was increased by conjugation with carbon nanotubes. Numbers presented in the two determined gates represent the percentage of cells in relation to the total cell number. (b,c) BALB/c mice were immunized with formulations containing OVA antigen and/or CpG oligonucleotides attached to carbon nanotubes or adsorbed onto alum. (b) ELISA plates coated with OVA were used to quantify the levels of OVA-specific total IgG, IgG1, and IgG2a isotypes present in sera of control and immunized mice. (c) Splenocytes from vaccinated mice were stimulated with T CD4⁺- or T CD8⁺-specific peptides or with OVA protein. IFN- γ production was measured by ELISA at 72 h after stimulation. Error bars show standard error of the mean. Statistical analyses were performed using one-way ANOVA with Bonferroni post-test.

supravital dye neutral red (NR assay, Sigma) and the reduction of tetrazolium salt by mitochondrial enzymes (MTT assay, Sigma). Each group was cultured in triplicates and then DCs were incubated with different amounts of oxidized MWCNTs (1, 10, 20, and 50 $\mu\text{g}\cdot\text{mL}^{-1}$). Results from both tests revealed the MWCNTs to have very low acute toxicity and we observed no significant changes in viability up to 20 $\mu\text{g}\cdot\text{mL}^{-1}$ (Supporting Information Figure S3b). Therefore, we used this concentration for all subsequent assays. This minimal toxic effect observed with the treated nanotubes was not unexpected because acid treatment removes the metal catalyst, which should substantially reduce the potential cytotoxic effect of the CNTs.^{39,43} The reduced length and high dispersibility of MWCNTs in aqueous solution acquired after functionalization process also could play a relevant role in enhancing

cytocompatibility.¹⁴ Furthermore, we used a standardized protocol for sample preparation, which allowed the manufacturing of MWCNTs with a high purity grade. The capacity to induce acute toxicity or oxidative stress of high concentrations of impurities like metals or amorphous carbon is well-known.⁴⁴

B Cell and T Cell-Mediated Immunity Induced by MWCNT Constructs. Having shown that MWCNTs constructs could be internalized by dendritic cells without affecting cellular viability, we next examined the capability of DCs loaded with MWCNTs complexes to stimulate OVA-specific T cells in vitro. Figure 4a shows the CFSE profiles of CFSE-labeled ovalbumin (OVA)-specific CD4⁺ and CD8⁺ T cells after 4 days culture with dendritic cells loaded with MWCNTs, OVA or MWCNT-OVA complex. As controls, T cells cultured with no stimulation show the CFSE intensity of nondivided cells. We

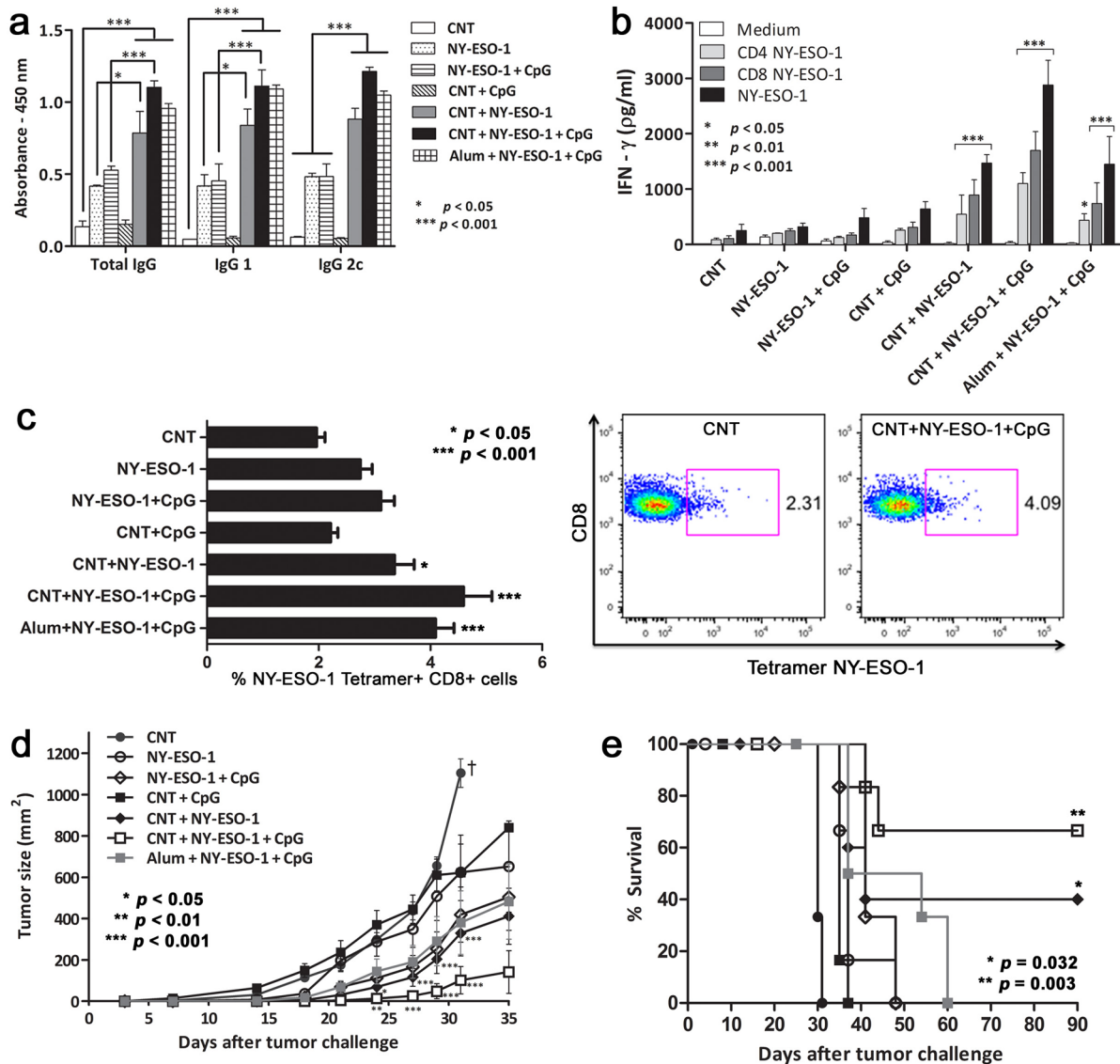


Figure 5. Carbon nanotubes-based antitumor formulation induced strong humoral and cellular specific immune response and protected mice against tumor development. (a,b) C57BL/6 mice were immunized with formulations containing the tumor-associated antigen NY-ESO-1 and/or CpG oligonucleotides noncovalently adsorbed to multiwalled carbon nanotubes or adsorbed onto alum. The specific antibody in sera of control and immunized mice (a) and IFN- γ production by splenocytes after stimulation with T CD4 $^+$ - or T CD8 $^+$ -specific peptides or with rNY-ESO-1 protein (b) was evaluated by ELISA. Vaccination with the antigen alone or mixed with alum did not induce such response. (c) Splenocytes from immunized mice were stained with anti-CD3, anti-CD8, and NY-ESO-1 tetramers and analyzed by flow cytometry. Representative dot plots and a graph summarizing the percentage of double-positive cells are shown at right and left, respectively. (d,e) Mice that received immunization with NY-ESO-1 were challenged with B16F10 transgenic melanoma expressing NY-ESO-1. Tumor growth (d) and survival (e) were monitored for 35 and 90 days, respectively. Error bars show standard errors of the mean.

detected a robust proliferative response for both CD4 $^+$ and CD8 $^+$ in MWCNTs-OVA stimulated cultures compared with the controls, as determined by protein uptake and efficient in vitro cross-presentation of OVA facilitated by MWCNT-based antigen delivery. In the nanotubes-antigen treated cultures, populations of CFSE-low CD3 $^+$ lymphocytes emerged, which represented 32.5 and 29.7% for CD4 $^+$ and CD8 $^+$ of the cells in culture, respectively. The results showed that even if the DCs function was preserved, as demonstrated by cytotoxicity assays, the specific T cell proliferation was minimal in the cells loaded with only MWCNT (7.68% for CD4 $^+$ and 5.87% for CD8 $^+$ T cells) or OVA (11.9% for CD4 $^+$ and 9.03% for CD8 $^+$ T cells) alone (Figure 4a). Consistent with our in vitro results, MWCNT constructs were also capable of enhancing CD4 $^+$

and CD8 $^+$ T cell proliferation in the peripheral circulation and splenic tissue of immunized mice.⁴⁵ These findings indicated that our nanoparticle-based formulation becomes particularly suitable for a vaccination purpose by providing a multiple signals necessary for both CD4 $^+$ T as well as CD8 $^+$ T cell expansion through APC activation.⁴⁶

We further tested the extent to which the internalized MWCNTs conjugated with ovalbumin could induce an antigen-specific immune response in vivo (Figure 4b,c). BALB/c mice were submitted to a protocol of three equivalent immunizations within an interval of 15 days. These immunizations were performed by the administration of 100 μ L of the vaccine formulation, subcutaneously. For each dose, 10 μ g of the immunogenic protein with addition or not of 18

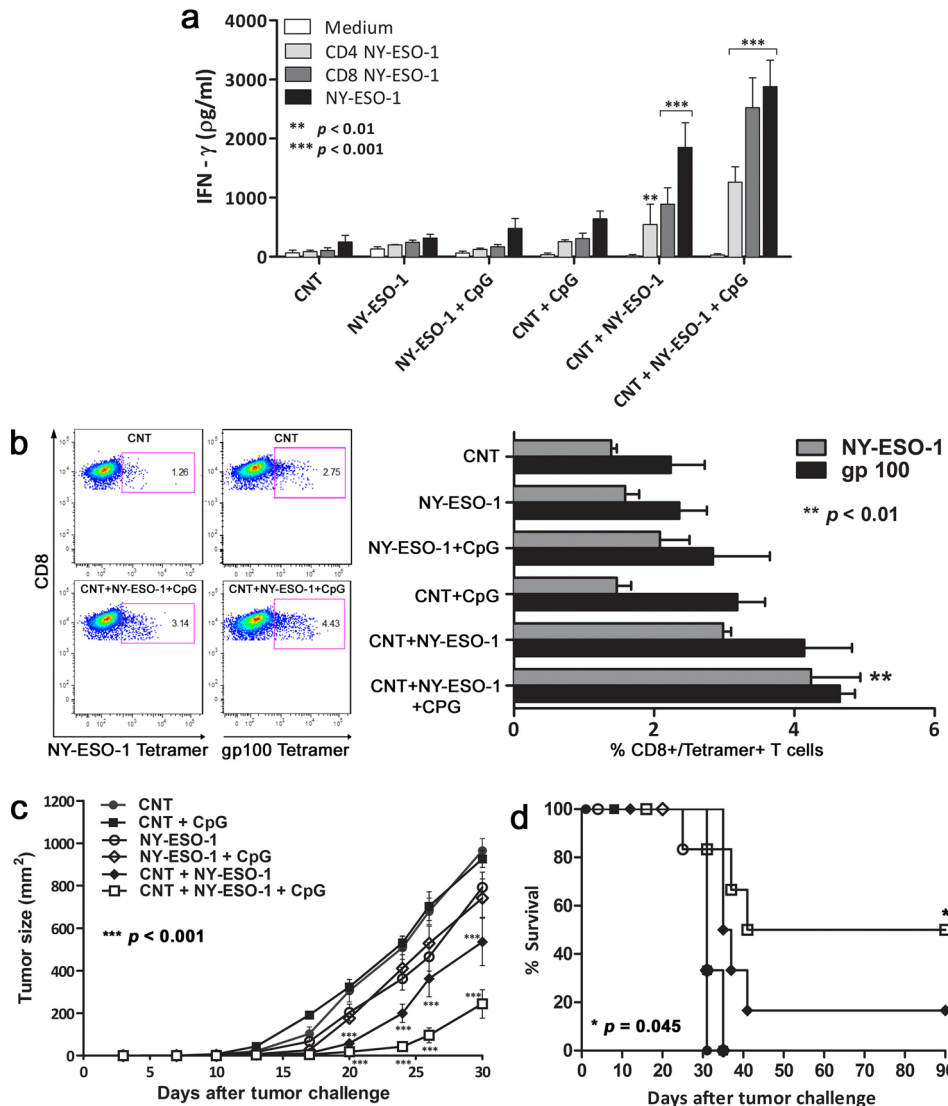


Figure 6. Therapeutic protocol using shortened oxidized MWCNTs delayed tumor growth expressing NY-ESO-1 and prolonged the survival in treated mouse. B16F10 -NY-ESO-1-bearing mice were treated with two doses of formulations containing or not containing CNTs given 7 days apart, starting at day 3 postchallenge. (a) The cellular immune response induced by the therapeutic protocol was assessed 21 days after the last dose and the IFN- γ production by splenocytes was measured by ELISA at 72 h after restimulation. (b) Before stimulation, the splenocytes were stained with anti-CD3, anti-CD8, and NY-ESO-1 or gp100 tetramers and analyzed by flow cytometry. Representative dot blots and a graph summarizing the percentage of double-positive cells are shown at left and right, respectively. Tumor growth (c) and survival (d) were monitored for 30 and 90 days, respectively.

μ g of CpG oligonucleotides (B-class-2.97 TCCTCGTTTGACGTG)⁴⁷ were added to 20 μ g of oxidized MWCNT in aqueous dispersion. The kinetics for both protein binding and synthetic adjuvant hybridization was accelerated by continuous sonication for 30 min.⁴⁸

To characterize T cell responses from immunized mice we examined their production of IFN- γ , a central cytokine that orchestrates T cell-mediated immunity against tumor cells. Splenocytes were stimulated *in vitro* with OVA-derived peptides that encode epitopes recognized by either CD4 $^{+}$ or CD8 $^{+}$ T lymphocytes. Our data demonstrated that immunization of mice with the model antigen (ovalbumin) adsorbed onto MWCNTs causes priming of T cell activation to a greater extent than immunization with OVA adsorbed onto alum, which is widely used as an adjuvant (Figure 4c). As a control, the protein alone did not show such response, indicating the good carrier ability of MWCNTs *in vivo*. These results are

consistent with other studies that suggest the differential properties of carbon nanotubes for stimuli presentation and antigen-specific T cell stimulation.⁴⁹ As expected, we noted that the antigen immunogenicity was greatly enhanced when allied to the combined delivery of synthetic CpG oligonucleotide. The group immunized with MWCNT-OVA-CpG constructs was more effective at generating OVA specific, IFN- γ -producing CD4 $^{+}$ and CD8 $^{+}$ T cells (Figure 4c). It is well-known that TLR9, a potent inducer of both innate and adaptive immune responses, is located intracellularly. Thereby, we assume that MWCNTs play a pivotal role in improving the immunostimulatory signal of CpG molecules by enhancing CpG oligonucleotides internalization by APCs.^{8,50}

To determine whether the nanoparticles complexes could also induce specific anti-OVA antibody production we measured antibody titers in serum 21 days after the last immunization. We found that the immunization with the

complete formulation containing OVA and CpG molecules, both adsorbed onto MWCNTs surfaces, substantially enhanced OVA-specific IgG antibody titers (Figure 4b). Taken together, our findings suggest that the larger amount of MWCNT-delivered CpG was able to trigger an strong intracellular signaling leading to the activation of the dendritic cells and B-cells, and the production of cytokines, chemokines, and immunoglobulins. Subsequently, cytokines produced by DCs, such as IL-12 (Supporting Information Figure S5), induced the differentiation of naive T cells into T helper 1 (Th1), as seen by the higher INF- γ secretion, as well as CD8 $^{+}$ T cells.

MWCNT-NY-ESO-1 Conjugates Induce Antigen-Specific Immunity and Tumor Inhibition in Mice. After confirming the potential activity of the MWCNTs-based formulation *in vivo*, they were tested in another system, aiming at their use as an antitumor vaccine. C57BL/6 mice were immunized with the new formulation, containing the same proportions of nanoparticle, antigen, and adjuvant as in immunizations with OVA. We used in this experiment two immunization doses 21 days apart. Our results demonstrate that formulations containing MWCNTs were more effective in stimulating the host immune system to mount an integrated humoral and cellular responses to NY-ESO-1 antigen (Figure 5a,b). We could also confirm the effective antigen specificity on the response of the CD8 $^{+}$ T lymphocytes to the tumor cells by evaluating the double positive CD8 and NY-ESO-1 tetramer T cells (Figure 5c). The increase in T cell responses resulted in a greater protection and prolonged survival of mice challenged with a syngeneic transgenic melanoma, the B16F10 cell line expressing NY-ESO-1, as compared with the formulations using the recombinant protein and CpG oligonucleotides adsorbed onto alum (Figure 5d,e).

We also tested the ability of all nanoformulations in a therapeutic protocol to reverse/delay tumor growth in B16-NY-ESO-1-bearing mice. Mice were challenged with melanoma cell line and 3 and 10 days later injected subcutaneously with MWCNT-based formulations. Nanotube-constructs vaccination induced both CD4 $^{+}$ T as well as CD8 $^{+}$ T lymphocytes to produce IFN- γ after restimulation with recombinant NY-ESO-1 or NY-ESO-1 specific peptides (Figure 6a). The latter results were confirmed by the increased frequency of CD8 $^{+}$ T lymphocytes, which reacted with the NY-ESO-1 tetramer. Furthermore, we found that the nanotubes-based treatment was able to induce spreading to other melanoma antigens beyond NY-ESO-1, as can be seen by the frequency of gp100 tetramer $^{+}$ cytolytic T cells (Figure 6b). We also report a delay in tumor growth and survival rate in mice treated with MWCNTs-NY-ESO-1-CpG formulation (Figure 5c,d).

We found very similar results with CT26, a colon carcinoma cell line expressing NY-ESO-1. Our formulation containing MWCNTs both inhibited and delayed tumor growth in prophylactic and therapeutic protocols, respectively (Supporting Information Figure S6).

Conclusions. In this study, we report the effectiveness of a fully synthetic supramolecule that allied the advantage of the shortened oxidized MWCNTs, as a vector in biology systems associated with a recombinant antigen and synthetic adjuvant, to efficiently target APCs and to induce strong CD8 $^{+}$ T cell mediated immunity. Facing the difficulties of finding an effective way to counterattack different cancer cells, our nanocomplex represents an important tool for *in vivo* intracellular dispensation and activation, even for more than one antigen simultaneously. This strategy could be applied in

diverse cross-presentation pathway-related protocols that need both humoral- and cell-mediated immune responses. The relative simplicity and low cost of fabrication of MWCNTs can indeed offer a highly attractive and promising alternative for prophylactic and therapeutic vaccines for cancer and infectious diseases.

Methods. *Synthesis and Oxidation of Multiwalled Carbon Nanotubes.* MWCNT was grown by chemical vapor deposition (CVD) at a growth temperature of 700 to 900 °C, using ethylene as carbon precursor gas and argon as carrying gas. The pyrolysis process was catalyzed by cobalt and iron oxide nanoparticles anchored to a magnesium oxide matrix. Residual amorphous carbon, metallic nanoparticles, and ceramic matrix were initially removed by thermal oxidation at 450 °C for 30 min and thereafter digestion in 37 vol % hydrochloric acid for 24 h. An additional oxidative treatment was performed in a 3:1 mixture of concentrated sulfuric and nitric acid under microwave-assisted reflux at a power of 500 W for 15 min, aiming at the shortening and functionalization of the tube extremities and walls with acid-oxygenated groups. The oxidized MWCNT sample was filtered in polycarbonate membrane and exhaustively base washed with a pH 11 NaOH solution to remove carboxylated carbon (CC) impurities that might have adsorbed onto the nanotube surface during the oxidation process. Then, it was dispersed in Milli-Q water at a concentration of 0.25 mg·mL⁻¹ after 60 min of direct tip sonication. At the end, an aqueous dispersion of multiwalled carbon nanotubes functionalized with similar amount of carboxylic acids and phenols (by acid base potentiometric titration), mostly up to 600 nm in length and with average diameter of 10–40 nm (by TEM) and approximate purity of 95% in mass (by thermogravimetry), was obtained.

Optical Absorption Spectroscopy. Optical absorption spectra were taken with a UVPC Shimadzu recording spectrometer over a wavelength range of 190–900 nm and a cell path length of 1 cm.

Raman Spectroscopy. A total of 2 × 10⁴ dendritic cells were incubated on poly-L-lysine-coated 4-well Lab-Tek Chamber Slide System (Nunc, Thermo Scientific), with 20 µg·mL⁻¹ of MWCNT, OVA, or MWCNT-OVA conjugated for 24 h at 37 °C. The chamber slides were washed twice with PBS and then cells were fixed with PBS containing 4% paraformaldehyde for 30 min at 4 °C. The micro-Raman imaging experiments were obtained using a Witec Alpha 300 instrument, operating with 532 nm laser line. Typical laser intensity and accumulation time are 10⁹ W/m² and 0.2 s, respectively. Raman imaging of several cells samples were obtained always in an area about 30 µm × 30 µm. To generate the images, G band, centered at 1585 cm⁻¹, was chosen and the Raman images always show only its intensity.

Transmission Electron Microscopy. TEM images were obtained in Tecnai G2-12-SpiritBiotwin-120 kV and Tecnai G2-20-SpiritBiotwin-200 kV equipment. For oxidized MWCNT and MWCNT-OVA-CpG, samples were dropped on copper grids covered with holey carbon film and dried at room temperature for 24 h. To measure the length distribution of the MWCNT being taken up by the cells, fixed DCs incubated with complexes MWCNT-OVA were stained with osmium tetroxide and uranyl acetate, dehydrated and embedded into an epoxy resin (Epon1 812). Ultrathin layers (90 nm thickness) were sliced with a diamond ultramicrotome and deposited on copper grids.

Animals and Immunizations. C57BL/6 and BALB/c mice were obtained from CEBIO (Federal University of Minas Gerais, Brazil). Six- to eight-week-old females, weight-matched, were used in the different experimental groups. Immunizations were performed by inoculating 100 μ L of the vaccine formulation into the right flank of mice, subcutaneously. For each dose, 10 μ g of the immunogenic protein (OVA or NY-ESO-1) with addition or not of 18 μ g of CpG oligonucleotides (Alpha DNA) were added to 20 μ g of oxidized MWCNT in aqueous dispersion. Positive controls were prepared with 10 μ g of the immunogenic protein and 18 μ g of CpG coadsorbed in 30% (v/v) of alum Rehydragel L.V. solution (Reheis) for 1 h at room temperature in a tube rotator. After incubation, saline solution was added to each sample to the final volume. Experiments for this study were approved by the Ethical Commission on Animals' Use (CETEA) at Federal University of Minas Gerais and performed following Institutional Guide for the Care and Use of Laboratory Animals.

Measurement of Antibody and T Cell Responses. Vaccinated and control mice were bled from the retro-orbital plexus under ether anesthesia. Antigen-specific antibodies were measured in sera from immunized mice by enzyme-linked immunosorbent assay (ELISA). Secondary Ab, peroxidase-conjugated goat antimouse total Immunoglobulin G (IgG), IgG1, and IgG2a (BALB/c) or IgG2c (C57BL/6) (SouthernBiotech) were used and the reactions were detected with 3,39,5,59-tetramethylbenzidine reagent (Sigma-Aldrich). For IFN- γ production assays, splenocytes from vaccinated mice were prepared in complete RPMI supplemented with 100 U·mL⁻¹ rIL-2 (R&D Systems), plated at 5 \times 10⁶ cells·mL⁻¹ and incubated at 37 °C and 5% CO₂ for 72 h in the presence or absence of epitopes derived from OVA or NY-ESO-1 proteins. IFN- γ concentrations were determined in cell culture supernatants with DuoSet ELISA (R&D Systems). For flow cytometry analysis, CD8⁺ T cells were stained with anti-CD8 mAb and MHC tetramers presenting specific epitope NY-ESO-1 or gp100 (LICR Tetramer Facility).

Flow Cytometry Analysis. Cells were processed and stained for surface molecules for 30 min at room temperature. The cells were washed and fixed in PBS with 2% paraformaldehyde. After incubation, cells were washed, permeabilized (Cytofix/Cytoperm, BD Biosciences), stained with intracellular molecules for 30 min at 4 °C, and then fixed in 200 μ L of PBS with 2% paraformaldehyde. At least 200 000-gated events were acquired for analysis using LSR II with Diva (BD Biosciences). The antibodies used for staining were anti-CD3-APC-Cy7, anti-CD4-AlexaFlour700, anti-CD8-PE-Cy7, anti-CD3-APC-Cy7, anti-CD11c-AlexaFlour700, anti-MHCII-APC, anti-B220-PerCP-Cy5.5, anti-CD11b-PE-Cy7, anti-GR-PerCP-Cy5.5, and anti-DX5-APC (eBioscience). FlowJo (v8.8.6) and GraphPad Prism (v5.0b) were used for data analysis and graphic presentation.

Tumor Challenge. B16-NY-ESO-1 melanoma and CT26-NY-ESO-1 colon carcinoma cell lines were grown at 37 °C under 5% CO₂ in complete RPMI 1640 (Sigma) with 100 U·mL⁻¹ penicillin and 100 μ g·mL⁻¹ streptomycin and supplemented with 10% heat inactivated fetal calf serum (FCS; GIBCO). The selection was performed with G418 (800 μ g·mL⁻¹). To establish subcutaneous tumors control and immunized mice were challenged with 5 \times 10⁴ B16-NY-ESO-1 or 10⁶ CT26-NY-ESO-1 cells in 100 μ L of PBS subcutaneously injected into the right flank. Mice were

followed up to 30 days for evaluation of tumor growth and survival was measured for 90 days.

Immunotherapy. C57BL/6 were challenged by subcutaneous injection with 5 \times 10⁴ NY-ESO-1-expressing B16F10 melanoma tumor cells, and BALB/c mice were challenged with 10⁶ of CT26-NY-ESO-1. Mice were treated with two doses of each MWCNT-based formulations, the same used in prophylactic protocols given 7 days apart, starting at day 3 after challenge. The percentages of survival were measured for 90 days and tumor size was scored by measuring perpendicular diameters for 30 days.

Generation of Dendritic Cells (DCs). Bone marrow was collected from tibias and femurs of female BALB/c mice, passed through a nylon mesh to remove small pieces of bone and debris, resuspended in complete medium (RPMI-1640 medium containing 10% fetal bovine serum, L-glutamine, penicillin/streptomycin, and 20 ng·mL⁻¹ mouse GM-CSF) and cultured in cell culture dishes at an initial density of 2 \times 10⁶ cells in 20 mL/plate. On days 3 and 6 of incubation, fresh medium with GM-CSF was either added or replaced half of the culture medium. On day 9 of culture, most of the nonadherent cells had acquired typical dendritic morphology, and these cells were used as the source of DC in subsequent experiments. For cellular viability assay, MWCNT-peptide uptake experiments, and microscopy, immature DCs were seeded into multiwell plates or coverglass bottom microscopy dishes and assayed as described. To determine the cytokine profile of CpG-loaded DCs, immature differentiated cell cultures were incubated at 37 °C and 5% CO₂ for 24 h with 18 μ g·mL⁻¹ of CpG ODNs coupled or not to different concentrations (10 or 20 μ g·mL⁻¹) of MWCNT. LPS was used as positive control. IL-12 and IL-10 concentrations were determined in cell culture supernatants with DuoSet ELISA (R&D Systems).

Cell Viability Determination. The viability of DCs was measured by using MTT and NR assays. Briefly, cells were seeded at a concentration of 5 \times 10⁵ cells in 24-well culture plate. After 24 h, culture with different concentrations of MWCNT (0, 1, 10, 20, and 50 μ g·mL⁻¹), 3-[4,5-dimethylthiazol-2-yl]-2,5-diphenyltetrazolium bromide (MTT, Sigma) was added at a concentration of 0.5 mg·mL⁻¹ and incubated at 37 °C in CO₂ for 2 h. Viable DCs generate insoluble crystal, but DCs are floating and loosely attached on the surface of culture plates. So, 100 μ L/well 10% SDS solution containing 0.01 N HCl was directly added into wells to avoid the potential loss of and dissolve the insoluble crystal generated by DCs. After 24 h, the absorbance of sample was measured at 570 nm by using microplate reader. Alternatively, at the end of the stimulation period, 0.33% of Neutral Red solution was added to each well, and the 96 well plate was further incubated for 4 h at 37 °C under 5% CO₂. At that time, 100 μ L of a fixative formal/calcium solution (0.1% CaCl₂ in 0.5% formaldehyde) was added for 1 min, followed by a solubilization solution of acetic acid/EtOH (1% acetic acid in 50% ethanol). Supernatant was then recovered, and the absorbance measured spectrophotometrically at a wavelength of 540 nm.

Confocal Microscopy. Immature bone marrow-derived (day 9) dendritic cells were loaded for 18 h with the constructs (MWCNT alone, FITC-labeled OVA peptide only, and with MWCNT-peptide complexes). Treated cells were then fixed with 4% paraformaldehyde (Sigma) and permeabilized with 0.2% Triton X-100 (Sigma). For assessment of colocalization studies in live cells, ER-Tracker Blue-White DPX (100 nM, Life Technologies), Lysotracker Red (100 nM, Life Technologies),

and AF633-Cholera toxin B ($10 \mu\text{g}\cdot\text{mL}^{-1}$, Life Technologies) was added for 30 min at 37°C . After incubation, the cells were rinsed off with a gentle PBS wash, the incubation buffer replaced, and observed using a Zeiss 5 Live confocal microscope equipped with 405 nm laser diode, 488 nm laser diode, diode-pumped solid-state laser 532 nm and laser diode 635 nm for confocal fluorescence microscopy using a $63\times$, 1.4 NA objective lens at 1–5 frames/s.

Migration of MWCNT-Peptide Complexes. A total of $10 \mu\text{g}$ of FITC-labeled OVA peptide adsorbed to $20 \mu\text{g}$ of MWCNT were inoculated subcutaneously. After 1 h, 20 h, and 3 days, the inguinal lymph nodes and spleen were harvested. The cells were processed and stained for the surface markers as described above. The presence of FITC-labeled constructs in macrophages ($\text{CD11b}^+ \text{GR1}^-$), dendritic cells ($\text{CD11c}^+ \text{MHCII}^{\text{high}}$), B lymphocytes (B220^+), NK cells (DX5^+), and T lymphocytes (CD3^+) was evaluated by flow cytometry.

Lymphocyte Proliferation Assay. In vitro cross-presentation of OVA was measured by a dye dilution assay of CFSE-labeled T cells. For splenic DC isolation, splenocytes from mice previous immunized with OVA were processed and the DC population enriched using EasySep CD11c positive selection (StemCell Technologies) according to the manufacturer's instructions. MWCNT ($20 \mu\text{g}\cdot\text{mL}^{-1}$), OVA ($10 \mu\text{g}\cdot\text{mL}^{-1}$), or MWCNT-OVA were incubated with $5 \times 10^4 \text{ CD11c}^+$ cells for 24 h. CD8^+ T and CD4^+ T cells were isolated from total splenocytes using Dynabeads (Invitrogen Dynal, Oslo, Norway) and stained with $1.25 \mu\text{M}$ CFSE at $1 \times 10^7 \text{ cells/mL}$ for 8 min. After incubation, DCs were washed three times, and coincubated at 37°C , 5% CO_2 . After 5 days of culture, the cells were stained with the following antibodies: anti-CD3-APC-Cy7, anti-CD4-FITC, anti-CD8-PE-Cy7, anti-MHCII-APC, anti-CD11c-Alexa 700, as described above.

Statistics. Statistic significance for ELISA and cytokine staining assays were evaluated using One-Way ANOVA and nonparametric test followed by Bonferroni post-test. Statistic significance for tumor growth was evaluated by two-way ANOVA with Bonferroni post-test.

■ ASSOCIATED CONTENT

Supporting Information

Additional figures and video as described in the text. This material is available free of charge via the Internet at <http://pubs.acs.org>.

■ AUTHOR INFORMATION

Corresponding Authors

*(R.T.G.) E-mail: ritoga@cpqrr.fiocruz.br. Tel: (0055) (31) 3349-7774. Fax: (0055) (31) 3295-3115.

*(C.A.F.) E-mail: clas@cdtn.br. Tel: (0055) (31) 3069-3162. Fax: (0055) (31) 3069-3390.

Author Contributions

○P.C.B.d.F., L.I.d.S., C.A.F., and R.T.G. contributed equally to this work.

Notes

The authors declare no competing financial interest.

■ ACKNOWLEDGMENTS

We thank Adelina Pinheiro Santos from Centro de Desenvolvimento da Tecnologia Nuclear and Cristiano Fantini from Federal University of Minas Gerais for scientific discussions and suggestions during the development of this

work; Mariana Botelho Barbosa from Centro de Desenvolvimento da Tecnologia Nuclear for help with MWCNT dispersions preparation; Kinulpe Honorato Sampaio from Microscopy Center of Federal University of Minas Gerais for scientific discussions and suggestions on TEM analyzes; Bruno Galvão Filho from Federal University of Minas Gerais for help with animal experiments; the LICR Tetramer Facility for tetramers synthesis; the LICR–Cornell University for the recombinant NY-ESO-1 protein; Dr. Jonathan Cebon from LICR–Melbourne for the B16-NY-ESO-1 cell line; and Dr. Hiroyoshi Nishikawa from Mie University Medical School for the CT26-NY-ESO-1 cell line. This study was funded by Fundação de Amparo à Pesquisa de Minas Gerais (FAPEMIG), Fundação Oswaldo Cruz, the National Institute of Science and Technology for Vaccines/Conselho Nacional de Desenvolvimento Científico e Tecnológico (CNPq), the National Institute of Science and Technology for Carbon Nanomaterials/CNPq, and the Nanotoxicology Network (CNPq process number 552131/2011-3). This work was also supported by NIH grant 1R03TW008709.

■ REFERENCES

- (1) Fabbro, C.; Ali-Boucetta, H.; Da Ros, T.; Kostarelos, K.; Bianco, A.; Prato, M. Targeting carbon nanotubes against cancer. *Chem. Commun.* **2012**, *48*, 3911–3926.
- (2) Desai, N. Challenges in development of nanoparticle-based therapeutics. *AAPS J.* **2012**, *14*, 282–95.
- (3) Villa, C. H.; Dao, T.; Ahearn, I.; Fehrenbacher, N.; Casey, E.; Rey, D. A.; Korontsvit, T.; Zakhaleva, V.; Batt, C. A.; Philips, M. R.; et al. Single-Walled Carbon Nanotubes Deliver Peptide Antigen into Dendritic Cells and Enhance IgG Responses to Tumor-Associated Antigens. *ACS Nano* **2011**, *5*, 5300–5311.
- (4) Pantarotto, D.; Partidos, C. D.; Hoebeke, J.; Brown, F.; Kramer, E.; Briand, J. P.; Muller, S.; Prato, M.; Bianco, A. Immunization with Peptide-Functionalized Carbon Nanotubes Enhances Virus-Specific Neutralizing Antibody Responses. *Chem. Biol.* **2003**, *10*, 961–966.
- (5) Pantarotto, D.; Briand, J. P.; Prato, M.; Bianco, A. Translocation of bioactive peptides across cell membranes by carbon nanotubes. *Chem. Commun.* **2004**, *7*, 16–17.
- (6) Han, Z. J.; Ostrikov, K. K.; Tan, C. M.; Tay, B. K.; Peel, S. A. Effect of hydrophilicity of carbon nanotube arrays on the release rate and activity of recombinant human bone morphogenetic protein-2. *Nanotechnology* **2011**, *22*, 295712.
- (7) Kam, N. W. S.; Dai, H. Carbon Nanotubes as Intracellular Protein Transporters: Generality and Biological Functionality. *J. Am. Chem. Soc.* **2005**, *127*, 6021–6026.
- (8) Zhao, D.; Alizadeh, D.; Zhang, L.; Liu, W.; Farrukh, O.; Manuel, E.; Diamond, D. J.; Badie, B. Carbon Nanotubes Enhance CpG Uptake and Potentiate Antiglioma Immunity. *Clin. Cancer Res.* **2011**, *17*, 771–782.
- (9) Pantarotto, D.; Singh, R.; McCarthy, D.; Erhardt, M.; Briand, J. P.; Prato, M.; Kostarelos, K.; Bianco, A. Functionalized carbon nanotubes for plasmid DNA gene delivery. *Angew. Chem., Int. Ed.* **2004**, *43*, 5242–5246.
- (10) Santosh, M.; Panigrahi, S.; Bhattacharyya, D.; Sood, A. K.; Maiti, P. K. Unzipping and binding of small interfering RNA with single walled carbon nanotube: a platform for small interfering RNA delivery. *J. Chem. Phys.* **2012**, *136*, 065106.
- (11) Ladeira, M. S.; Andrade, V. A.; Gomes, E. R.; Aguiar, C. J.; Moraes, E. R.; Soares, J. S.; Silva, E. E.; Lacerda, R. G.; Ladeira, L. O.; Jorio, A.; et al. Highly efficient siRNA delivery system into human and murine cells using single-wall carbon nanotubes. *Nanotechnology* **2010**, *21*, 385101.
- (12) Liu, Z.; Chen, K.; Davis, C.; Sherlock, S.; Cao, Q.; Chen, X.; Dai, H. Drug delivery with carbon nanotubes for in vivo cancer treatment. *Cancer Res.* **2008**, *68*, 6652–6660.

- (13) Wu, W.; Wieckowski, S.; Pastorin, G.; Benincasa, M.; Klumpp, C.; Briand, J. P.; Gennaro, R.; Prato, M.; Bianco, A. Targeted delivery of amphotericin B to cells by using functionalized carbon nanotubes. *Angew. Chem., Int. Ed.* **2005**, *44*, 6358–6362.
- (14) Bianco, A.; Kostarelos, K.; Prato, M. Applications of carbon nanotubes in drug delivery. *Curr. Opin. Chem. Biol.* **2005**, *9*, 674–679.
- (15) Wu, Y.; Phillips, J. A.; Liu, H.; Yang, R.; Tan, W. Carbon Nanotubes Protect DNA Strands during Cellular Delivery. *ACS Nano* **2008**, *2*, 2023–2028.
- (16) Bolhassani, A.; Safaiyan, S.; Rafati, S. Improvement of different vaccine delivery systems for cancer therapy. *Mol. Cancer* **2011**, *7*, 3.
- (17) Huleatt, J. W.; Jacobs, A. R.; Tang, J.; Desai, P.; Kopp, E. B.; Huang, Y.; Song, L.; Nakaar, V.; Powell, T. J. Vaccination with recombinant fusion proteins incorporating Toll-like receptor ligands induces rapid cellular and humoral immunity. *Vaccine* **2007**, *25*, 763–775.
- (18) Wille-Reece, U.; Flynn, B. J.; Loré, K.; Koup, R. A.; Kedl, R. M.; Mattapallil, J. J.; Weiss, W. R.; Roederer, M.; Seder, R. A. HIV Gag protein conjugated to a Toll-like receptor 7/8 agonist improves the magnitude and quality of Th1 and CD8+ T cell responses in nonhuman primates. *Proc. Natl. Acad. Sci. U.S.A.* **2005**, *102*, 5190–5194.
- (19) Chen, Y. T.; Ross, D. S.; Chiu, R.; Zhou, X. K.; Chen, Y. Y.; Lee, P.; Hoda, S. A.; Simpson, A. J.; Old, L. J.; Caballero, O.; et al. Multiple cancer/testis antigens are preferentially expressed in hormone-receptor negative and high-grade breast cancers. *PLoS One* **2001**, *6*, e17876.
- (20) Almeida, L. G.; Sakabe, N. J.; deOliveira, A. R.; Silva, M. C.; Mundstein, A. S.; Cohen, T.; Chen, Y. T.; Chua, R.; Gurung, S.; Gnjatic, S.; et al. CT database: a knowledge-base of high-throughput and curated data on cancer-testis antigens. *Nucleic Acids Res.* **2009**, *37*, D816–819.
- (21) Jungbluth, A. A.; Chen, Y. T.; Stockert, E.; Busam, K. J.; Kolb, D.; Iversen, K.; Coplan, K.; Williamson, B.; Altorki, N.; Old, L. J. Immunohistochemical analysis of NY-ESO-1 antigen expression in normal and malignant human tissues. *Int. J. Cancer* **2001**, *92*, 856–860.
- (22) Hemminger, J. A.; Ewart Toland, A.; Scharschmidt, T. J.; Mayerson, J. L.; Kraybill, W. G.; Guttridge, D. C.; Iwenofu, O. H. The cancer-testis antigen NY-ESO-1 is highly expressed in myxoid and round cell subset of liposarcomas. *Mod. Pathol.* **2013**, *26*, 282–288.
- (23) Jäger, E.; Chen, Y. T.; Drijfhout, J. W.; Karbach, J.; Ringhoffer, M.; Jäger, D.; Arand, M.; Wada, H.; Noguchi, Y.; Stockert, E.; et al. Simultaneous humoral and cellular immune response against cancer-testis antigen NY-ESO-1: definition of human histocompatibility leukocyte antigen (HLA)-A2-binding peptide epitopes. *J. Exp. Med.* **1998**, *187*, 265–270.
- (24) Kakimi, K.; Isobe, M.; Uenaka, A.; Wada, H.; Sato, E.; Doki, Y.; Nakajima, J.; Seto, Y.; Yamatsuji, T.; Naomoto, Y.; et al. A phase I study of vaccination with NY-ESO-1f peptide mixed with Picibanil OK-432 and Montanide ISA-51 in patients with cancers expressing the NY-ESO-1 antigen. *Int. J. Cancer* **2011**, *129*, 2836–2846.
- (25) Nicholaou, T.; Chen, W.; Davis, I. D.; Jackson, H. M.; Dimopoulos, N.; Barrow, C.; Browning, J.; Macgregor, D.; Williams, D.; Hopkins, W.; et al. Immunoediting and persistence of antigen-specific immunity in patients who have previously been vaccinated with NY-ESO-1 protein formulated in ISCOMATRIX. *Cancer Immunol. Immunother.* **2011**, *60*, 1625–1637.
- (26) Zhu, M.; Nie, G.; Meng, H.; Xia, T.; Nel, A.; Zhao, Y. Physicochemical properties Determine Nanomaterial Cellular Uptake, Transport, and Fate. *Acc. Chem. Res.* **2013**, *46*/3, 622–631.
- (27) Liu, J.; Rinzler, A. G.; Dai, H.; Hafner, J. H.; Bradley, R. K.; Boul, P. J.; Lu, A.; Iverson, T.; Shelimov, K.; Huffman, C. B.; et al. Fullerene pipes. *Science* **1998**, *280*, 1253–1256.
- (28) Kim, U. J.; Furtado, C. A.; Liu, X.; Chen, G.; Eklund, P. C. Raman and IR Spectroscopy of Chemically Processed Single-Walled Carbon Nanotubes. *J. Am. Chem. Soc.* **2005**, *127*, 15437–15445.
- (29) Ge, C.; Du, J.; Zao, L.; Wang, L.; Liu, Y.; Li, G.; Yang, Y.; Zhou, R.; Zhao, Y.; Chai, Z.; Chen, C. Binding of blood proteins to carbon nanotubes reduces cytotoxicity. *Proc. Natl. Acad. Sci. U. S. A.* **2011**, *108*/41, 16968–16973.
- (30) Sun, Z.; Nicolosi, V.; Rickard, D.; Bergin, S. D.; Aherne, D.; Coleman, J. N. Quantitative Evaluation of Surfactant-Stabilized Single-Walled Carbon Nanotubes: Dispersion Quality and Its Correlation with Zeta Potential. *J. Phys. Chem. C* **2008**, *112*, 10692–10699.
- (31) Chou, P. J.; Johnson, W. C. Base Inclinations in Natural and Synthetic DNAs. *J. Am. Chem. Soc.* **1993**, *115*, 1205–1214.
- (32) Hughes, M. E.; Brandin, E.; Golovchenko, J. A. Optical Absorption of DNA-Carbon Nanotube Structures. *Nano Lett.* **2007**, *7*/S, 1191–1194.
- (33) Zheng, M.; Jagota, A.; Semke, E. D.; Diner, B. A.; Mclean, R. S.; Lustig, S. R.; Richardson, R. E.; Tassi, N. G. DNA-assisted dispersion and separation of carbon nanotubes. *Nat. Mat* **2003**, *2*, 338–342.
- (34) Bloomfield, V. A.; Crothers, D. M.; Tinoco, I., Jr. Nucleic Acids: structures, properties and functions; University Science Books; Sausalito, CA, 2000; p 173.
- (35) Mu, Q.; Liu, W.; Xing, Y.; Zhou, H.; Li, Z.; Zhang, Y.; Ji, L.; Wang, F.; Si, Z.; Zhang, B.; Yan, B. Protein Binding by Functionalized Multiwalled Carbon Nanotubes Is Governed by the Surface Chemistry of Both Parties and the Nanotube Diameter. *J. Phys. Chem. C* **2008**, *112*, 3300–3307.
- (36) Kagan, V. E.; Konduru, N. V.; Feng, W.; Allen, B. L.; Conroy, J.; Volkov, Y.; Vlasova, I. I.; Belikova, N. A.; Yanamala, N.; Kapralov, A.; et al. Carbon nanotubes degraded by neutrophil myeloperoxidase induce less pulmonary inflammation. *Nat. Nanotechnol.* **2010**, *5*, 354–359.
- (37) Jain, S.; Singh, S. R.; Pillai, S. Toxicity Issues Related to Biomedical Applications of Carbon Nanotubes. *J. Nanomed. Nanotechol.* **2012**, *3*, 140.
- (38) Kam, N. W.; Liu, Z.; Dai, H. Carbon nanotubes as intracellular transporters for proteins and DNA: an investigation of the uptake mechanism and pathway. *Angew. Chem., Int. Ed.* **2006**, *45*, 577–581.
- (39) Porter, A. E.; Gass, M.; Bendall, J. S.; Muller, K.; Goode, A.; Skepper, J. N.; Midgley, P. A.; Welland, M. Uptake of Noncytotoxic Acid-Treated Single-Walled Carbon Nanotubes into the Cytoplasm of Human Macrophage Cells. *ACS Nano* **2009**, *3*, 1485–1492.
- (40) Randolph, G. J.; Angeli, V.; Swartz, M. A. Dendritic-cell trafficking to lymph nodes through lymphatic vessels. *Nat. Rev. Immunol.* **2005**, *5*, 617–628.
- (41) Pack, D. W. Timing is everything. *Nat. Mater.* **2004**, *3*, 133–134.
- (42) Bertulli, C.; Beeson, H. J.; Hasan, T.; Huang, Y. Y. Spectroscopic characterization of protein-wrapped single-wall carbon nanotubes and quantification of their cellular uptake in multiple cell generations. *Nanotechnology* **2013**, *24*, 265102.
- (43) Dumortier, H. Functionalized Carbon Nanotubes Are Non-Cytotoxic and Preserve the Functionality of Primary Immune Cells. *Nano Lett.* **2006**, *6*, 1522–1528.
- (44) Wörle-Knirsch, J. M.; Pulskamp, K.; Krug, H. F. Oops They Did It Again! Carbon Nanotubes Hoax Scientists in Viability Assays. *Nano Lett.* **2006**, *6*, 1261–1268.
- (45) Mocan, T.; Iancu, C. Effective colon cancer prophylaxis in mice using embryonic stem cells and carbon nanotubes. *Int. J. Nanomedicine* **2011**, *6*, 1945–1954.
- (46) Reddy, S. T.; van der Vlies, A. J.; Simeoni, E.; Angeli, V.; Randolph, G. J.; O’Neil, C. P.; Lee, L. K.; Swartz, M. A.; Hubbell, J. A. Exploiting lymphatic transport and complement activation in nanoparticle vaccines. *Nat. Biotechnol.* **2007**, *25*, 1159–1164.
- (47) Junqueira, C.; Guerrero, A. T.; Galvão-Filho, B.; Andrade, W. A.; Salgado, A. P.; Cunha, T. M.; Ropert, C.; Campos, M. A.; Penido, M. L.; Mendonça-Previato, L.; et al. Trypanosoma cruzi adjuvants potentiate T cell-mediated immunity induced by a NY-ESO-1 based antitumor vaccine. *PLoS One* **2012**, *7*, e36245.
- (48) Yang, R.; Tang, Z.; Yan, J.; Kang, H.; Kim, Y.; Zhu, Z.; Tan, W. Noncovalent Assembly of Carbon Nanotubes and Single-Stranded DNA: An Effective Sensing Platform for Probing Biomolecular Interactions. *Anal. Chem.* **2008**, *80*, 7408–7413.
- (49) Fadel, T. R.; Li, N.; Shah, S.; Look, M.; Pfefferle, L. D.; Haller, G. L.; Justesen, S.; Wilson, C. J.; Fahmy, T. M. Adsorption of multimeric T cell antigens on carbon nanotubes: effect on protein

structure and antigen-specific T cell stimulation. *Small* **2013**, *9*, 666–672.

(50) Bianco, A.; Hoebelke, J.; Godefroy, S.; Chaloin, O.; Pantarotto, D.; Briand, J. P.; Muller, S.; Prato, M.; Partidos, C. D. Cationic Carbon Nanotubes Bind to CpG Oligodeoxynucleotides and Enhance Their Immunostimulatory Properties. *J. Am. Chem. Soc.* **2005**, *127*, 58–59.